WM16

19th International Symposium of Ballistics, 7–11 May 2001, Interlaken, Switzerland

USING A NUMERICAL FRAGMENTATION MODEL TO UNDERSTAND THE FRACTURE AND FRAGMENTATION OF NATURALLY FRAGMENTING MUNITIONS OF DIFFERING MATERIALS AND GEOMETRIES

L.T. Wilson[1], D.R. Reedal[1], L.D. Kuhns[1], D.E. Grady[2], M.E. Kipp[3]

[1] *Naval Surface Warfare Center, Dahlgren Division, Dahlgren, VA*
[2] *Applied Research Associates, Inc., Albuquerque, NM*
[3] *Sandia National Laboratories, Albuquerque, NM*

Using an energy based fragmentation model implemented in the CTH shock physics code, we estimate the fragmentation characteristics of naturally fragmenting cylinders of several different materials and geometries. We look at the fracture of 4140 steel, a 70% tungsten alloy, tantalum, AerMet 100 steel and a 90% tungsten alloy, and examine the effects of scaling and material condition on our ability to accurately model fragmentation. These estimates are then compared to experimental data. This work illustrates the flexibility of the numerical fragmentation model and addresses its capability as a predictive tool.

BACKGROUND

Understanding the fracture and fragmentation of explosively loaded devices has been the focus of investigations for many years [1,2,3]. Much of the work has concentrated upon understanding the underlying physical mechanisms that govern breakup [4]. The efforts of Grady and Kipp have resulted in the implementation of a numerical fragmentation model in the CTH shock physics code [5,6]. In this model, the average fragment size, S, is given by

$$S = \left(\frac{\sqrt{24} K_f}{\rho \, c \, \dot{\varepsilon}} \right)^{2/3} \tag{1}$$

From Equation 1, we can see that the characteristic fragment size depends upon K*f*, a fragmentation constant; ρ, the material density; c, the sound speed; and ε, strain rate [4]. Using this model, we have been able to successfully replicate two fragmentation experiments [6], exploring the natural fragmentation of two materials, a 90% tungsten heavy alloy, and a high-strength steel alloy, AerMet100 in heat-treated condition. Using an experimentally determined fragmentation toughness, K*f*, and average fragment mass, we were able to reproduce the fragment mass cumulative distributions resulting from the detonation of explosively loaded cylinders like that shown in Figure 1 [6].

Figure 1: A Cylinder Expanding due to the Detonatiom of an Explosive Charge.

This paper examines the ability of the same model to estimate the fragmentation characteristics of naturally fragmenting munitions composed of several very different materials. We extend our previous work by addressing the fracture and breakup of explosively loaded cylinders composed of 4140 steel, a 70% tungsten alloy, tantalum, and AerMet® 100 in "as received" condition. We will also study the effect of scaling on our ability to accurately model fragmentation. In addition to providing fragmentation toughness constants for these materials and their breakup characteristics, we also estimate the fragment cumulative mass distributions. These estimates are then compared to experimental data. The objectives of this effort are to further illustrate the robust nature of the numerical fracture model as implemented in CTH and assess its capability as a predictive tool.

Technical Approach

The four materials used in this study were selected because they vary significantly from each other in terms of composition, ductility, and strength-characteristics that greatly affect material breakup.

We conducted 20 cm cylinder tests (detonating an explosive load inside cylinders nominally 20 cm by 20 cm, with a charge-to-metal mass (C/M) ratio of about one) to assess the fragmentation qualities of these materials. From these tests, we found an average fragment mass for each material based upon an exponential fit to the data [7]. Using this data, and a characteristic strain rate estimated using CTH calculations of the experiments, we were able to calculate fragmentation toughness from Equation (1). We then used the fragmentation toughness value as an input parameter for the numerical fragmentation model and re-ran CTH with actual test geometry. Following the calculation, we smoothed the CTH results using a post-processing technique that applied a Poisson distribution to the discrete fragment bins generated by CTH which were then summed to give an overall statistical distribution for the fragment mass. Finally, we compared this calculated distribution to the fragment mass distribution from the cylinder tests. This same process was used to evaluate the effects of scaling the test hardware, using a 10 cm by 10 cm, half-scale cylinder and a 10 cm by 20 cm, thick-walled cylinder.

Test Description and Results

Each test was instrumented with a high-speed framing camera and flash radiography. The framing camera was used to compare the amount of case expansion before rupture, and the radiography allowed us to determine fragment velocities and the velocity distribution. A soft recovery system of Vermiculite, attapulgite clay, and Celotex was used to recover the fragments, providing a means to determine the fragment mass distribution of each cylinder [8].

Figure 2 shows the test hardware configuration. The wall thickness for each test varied due to the difference in material density.

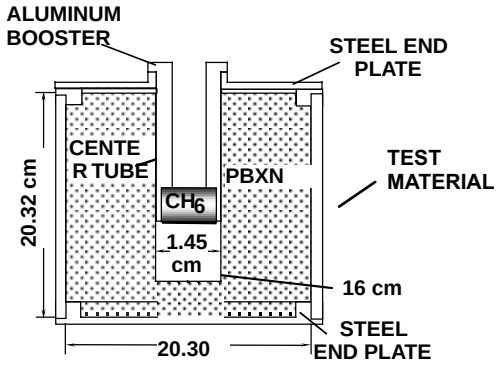

Figure 2: Test Hardware.

The results of the test series are covered in detail in Reference 7. The critical results for use with the Grady-Kipp fragmentation model are the average fragment size based upon an exponential fit of the data, given in Table 1, and the fragment mass distribution, which is discussed in more detail later.

Table 1: Average Fragment Mass

Material	Fragment Mass (grains)	Fragmentation Toughness ($m^{0.5}$MPa)
4140 steel	69.4	68
70% Tungsten	13.3	35
Tantalum	41.2	49

Solving Equation (1) for K*f* in terms of material properties, average fragment size, and a strain rate determined from CTH output yields Equation (2). Calculated values for fragmentation toughness, K*f*, are included in Table 1.

$$K_f := \sqrt{\frac{\rho\, c^2\, \varepsilon^2\, \mu}{24}} \tag{2}$$

Calculation Setup and Results

We performed detailed axisymmetric CTH runs using a minimum of 5 cells across the cylinder walls. The calculations were performed using a reactive burn model for the High explosive. Case materials were modeled using Mie Gruneisen equations of state and elastic perfectly plastic constitutive models. In order to trigger the fragmentation calculation in CTH, the fracture model uses the Johnson-Cook failure model as a two-parameter pressure dependent strain to failure model [6]. Figure 3 shows a sample setup.

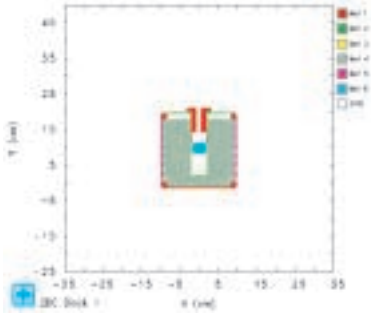

Figure 3: CTH Sample Set-up.

Figures 4, 5 and 6 show results from CTH and the corresponding experimental data for each material. Figures 4A, 5A, and 6A illustrate the calculated case expansion.

Figure 4: 4140 Steel Results.

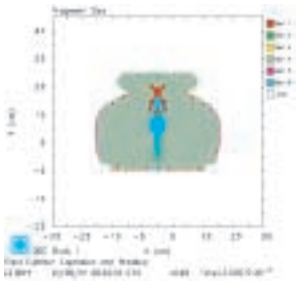

A: Late-Time Material Expansion

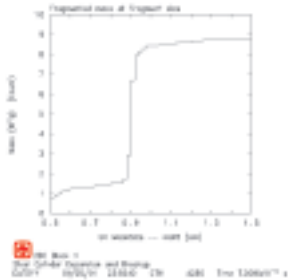

B: Cumulative Fragment Size Distribution

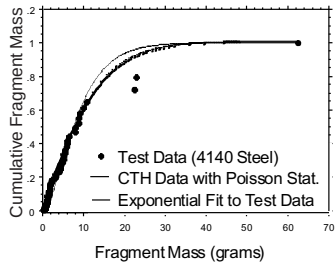

C: Cumulative Fragment Mass Dist. Comparison

Figure 5: 70% Tungsten Results.

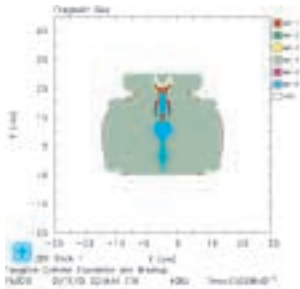

A: Late-Time Material Expansion

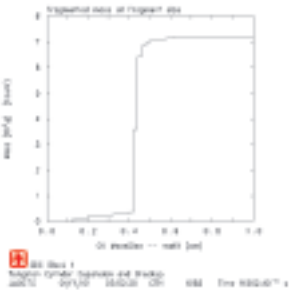

B: Cumulative Fragment Size Distribution

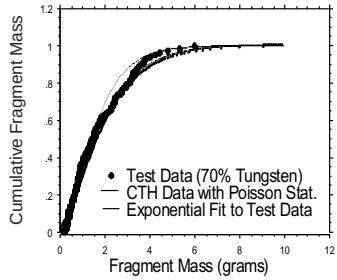

C: Cumulative Fragment Mass Dist. Comparison

Figure 6: Tantalum Results.

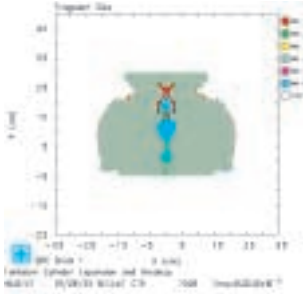

A: Late-Time Material Expansion

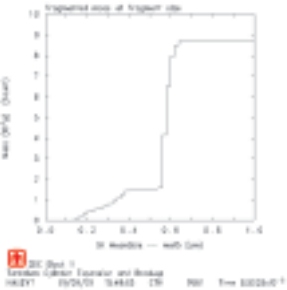

B: Cumulative Fragment Size Distribution

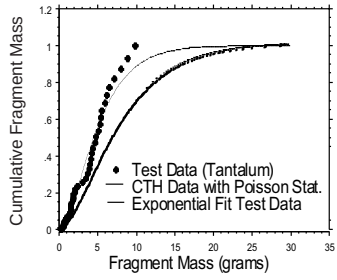

C: Cumulative Fragment Mass Dist. Comparison

Figures 4B, 5B, and 6B show the "raw" CTH cumulative distribution. Note in all cases that the "raw" CTH results indicate that most of the case mass would break into a very small number of fragment bin sizes. This result is consistent with our previous study, and is most likely due to the fact that the circumferential strain rate is almost constant in this test configuration [6]. The Grady-Kipp cumulative fragment mass distribution, with Poisson distribution post-processing, overlays the test data in Figures 4C, 5C and 6C. Reference 6 describes the concept of applying Poisson statistics to the fragment size bins calculated using CTH. The data from the 4140 steel cylinder test matches the CTH fragment mass distribution extremely well for the fragments below 200 grains. The test data and CTH results begin to diverge there, but the exponential curve fit to the test data remains close to the CTH results. The comparison for the 70% tungsten shows an exceptionally close match. Of the three materials tested, the tantalum test data and calculation results show the weakest correlation. Note in this case, however, that the characteristic fragment size obtained form CTH exceeds the wall thickness of the tantalum cylinder. This result, due to the fact that the fragmentation model as implemented in the code assumes the fragment aspect ratio is one – i.e., a cube – is clearly non-physical. Note also that the thin wall thickness of the tantalum case will bias the fragment distribution observed in the test.

Previous Test and Calculation Comparison

In conjunction with the tests detailed above, we conducted two 8-inch cylinder tests using AerMet® 100, a high-strength steel, in two material conditions – heat-treated and "as received." The heat-treated results were shown previously [6], but are shown in Figure 7 along with the "as received" results for completeness. The CTH results correspond very closely to the test data for the heat-treated Aermet® 100, and slightly less well for the "as received" material.

Figure 7: Comparison of Cumulative Fragment Mass Distribution from Test Data and CTH/Grady-Kipp Calculation for Aermet 100 in Two Material Conditions.

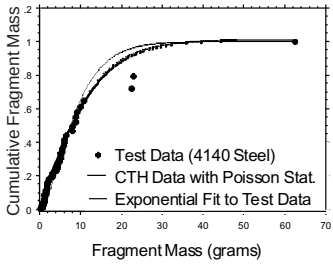

A: Aermet 100, heat-treated

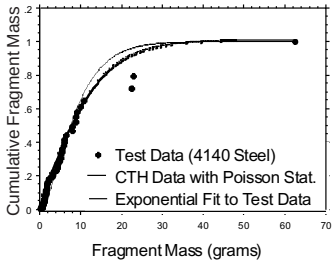

B: Aermet 100, "as received"

Scaling Effects

Finally, we also tested Aermet® 100 cylinders of two different scales. The tests are described in detail elsewhere in these proceedings. We looked at half-scale cylinders, 10 cm by 10 cm, with a C/M of about one. The second geometry we examined was a thick-walled cylinder, 10 cm in diameter with a 20 cm length. The unit had a wall thickness of 1.5 cm, and a C/M of 0.2.

The CTH calculations of these expanding cylinder tests used the same material properties and material parameters that were used for the 20 cm AerMet® 100 calculations. Figure 8 shows a comparison of calculation and test results. The half-scale CTH results vary greatly from the test data with the CTH results producing fragments of larger size than those observed in the tests. This is in agreement with observations made in a companion paper in these proceedings that show the fragmentation model will not accurately reproduce replica-scaling results in its current form. On the other hand, the thick-walled results match very closely, both in the overlay of the data and the exponential fit to the test data.

Figure 8: Comparison of Cumulative Fragment Mass Distribution Test Data and Calculation Results, for Scaled Aermet Cylinder Tests.

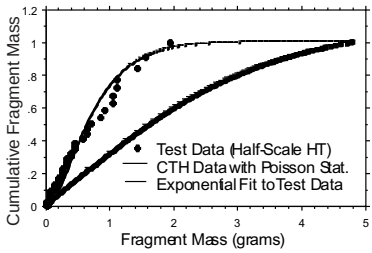

A: 10 cm by 10 cm, half-scale heat-treated

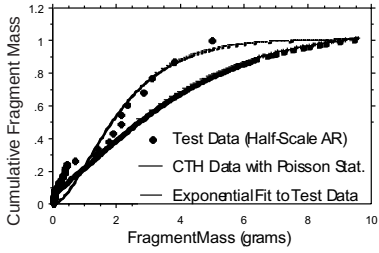

B: 10 cm by 10 cm, half-scale "as received"

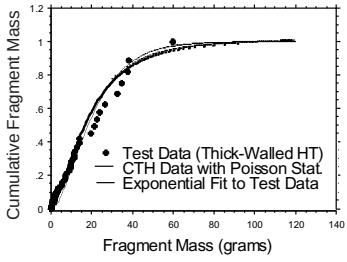

C: 10 cm by 20 cm, thick-walled heat-treated

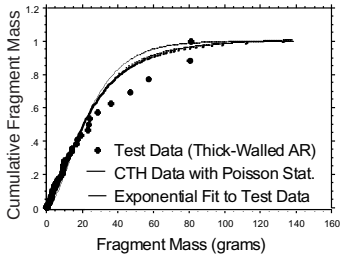

D: 10 cm by 20 cm, thick-"as received"

Conclusions

The Grady-Kipp fragmentation model, coupled with Poisson statistics, shows great ability to reproduce test results in terms of fragment mass distributions. It proved to be excellent in modeling the breakup of 4140 steel, 70% tungsten, and thick-walled Aermet® 100, and reasonable in matching the data from 8-inch Aermet® 100 tests.

Scaling appears to affect fragmentation in a way that is not fully accounted for by the fragmentation model, as the cumulative fragment mass distributions for the half-scale Aermet® cylinders are poorly approximated by the model. Material heat-treat condition seems to have minimal effect on the correlation between the model and the test data.

Overall, this numerical fracture model is fairly robust as implemented in CTH. For this work, the model was exercised after the tests were conducted, but the model shows potential for strong predictive capability.

REFERENCES

1. Mott, N. F. (1943). *"A Theory of the Fragmentation of Shells and Bombs"*, British Ministry of Supply Report A. C. 4035.
2. Mock, W. and Holt, W. H. (1983). *"Fragmentation Behavior of Armco Iron and HF-1 Steel Explosive-Filled Cylinders"*, J. Appl. Phys., 54, 2344–2351.
3. Grady, D. E. (1988). *"The Spall Strength of Condensed Matter"*, J. Mech. Phys. Solids, 36, 353–384.
4. Grady, D. E. and Kipp, M. E. (1985). *"Geometric Statistics and Dynamic Fragmentation"*, J. Appl. Phys., 58, 1210–1222.
5. McGlaun, J. M.; Thompson, S. L.; Elrick, M. G. (1990). *"CTH: A Three-Dimensional Shock Wave Physics Code"*, Int. J. Impact Engng, 10, 351–360.
6. Wilson, L. T.; Reedal, D. R.; Kipp, M. E.; Martinez, R. R.; and, Grady, D. E., *"Comparison of Calculated and Experimental Results of Fragmenting Cylinder Experiments"* for Explomet 2000, Fundamental Issues and Applications of Shock-Wave and High Strain-Rate Phenomena, Albuquerque, NM, June 19–22, 2000.
7. Rice, Donna J.; Kreider, Wayne; Garnett, Charles; and Wilson, Leonard T.; *"Comparing Fragmentation Characteristics of Tungsten, Tantalum and Steel"* for the 16th International Symposium on Ballistics Fragmentation, San Francisco CA, September 1996
8. Chhabildas, Lalit; Reinhart, William; Wilson, L. T.; Reedal, Donna R.; Grady, D. E.; and, Black, J. W., *Fragmentation Properties of AerMet®100 Steel in Two Material Conditions*, 19th International Symposium on Ballistics, Interlaken, Switzerland, 7–11 May 2001